



# Extracellular Nucleosomes Accelerate Microglial Inflammation via C-Type Lectin Receptor 2D and Toll-Like Receptor 9 in mPFC of Mice With Chronic Stress

Huanghui Wu<sup>1</sup>, Han Bao<sup>1</sup>, Cong Liu<sup>1</sup>, Qiao Zhang<sup>1</sup>, Ailing Huang<sup>1</sup>, Minxue Quan<sup>1</sup>, Chunhui Li<sup>1</sup>, Ying Xiong<sup>1</sup>, Guozhong Chen<sup>2\*</sup> and Lichao Hou<sup>1\*</sup>

<sup>1</sup> Department of Anesthesiology, Xiang'an Hospital of Xiamen University, School of Medicine, Xiamen University, Xiamen, China, <sup>2</sup> Department of Anesthesiology and Perioperative Medicine, Shanghai Fourth People's Hospital Affiliated to Tongji University, Shanghai, China

## OPEN ACCESS

### Edited by:

Jianguo Wu,  
Wuhan University, China

### Reviewed by:

Sagar Gaikwad,  
University of Texas Medical Branch at  
Galveston, United States

Venkata Surya Narayana Murty  
Darisipudi,  
University Medical Center Greifswald,  
Germany

### \*Correspondence:

Guozhong Chen  
cgzssq2000@sina.com  
Lichao Hou  
lchou@xah.xmu.edu.cn

### Specialty section:

This article was submitted to  
Inflammation,  
a section of the journal  
Frontiers in Immunology

**Received:** 13 January 2022

**Accepted:** 27 May 2022

**Published:** 29 June 2022

### Citation:

Wu H, Bao H, Liu C, Zhang Q,  
Huang A, Quan M, Li C, Xiong Y,  
Chen G and Hou L (2022) Extracellular  
Nucleosomes Accelerate Microglial  
Inflammation via C-Type Lectin  
Receptor 2D and Toll-Like Receptor 9  
in mPFC of Mice With Chronic Stress.  
*Front. Immunol.* 13:854202.  
doi: 10.3389/fimmu.2022.854202

Damage-associated molecular patterns (DAMPs) are the primary promoter of progressive neuroinflammation and are associated with chronic stress-related emotional disorders. The present study investigated the role and mechanism of extracellular nucleosomes and histones, the newly defined DAMPs, in mice with chronic stress. C57BL/6 mice were exposed to chronic unpredictable mild stress (CUMS) and corticosterone drinking, respectively, for 4 weeks. Negative emotional behaviors were comprehensively investigated. Microglial morphology, oxidative stress, and inflammation, as well as C-type lectin receptor 2D (Clec2d) and Toll-like receptor 9 (TLR9) expression in medial prefrontal cortex (mPFC) were assessed with flow cytometer and cell sorting. Specifically, microglial pro-inflammatory activation and inflammation were further investigated with stereotactic injection of recombinant nucleosomes and histones in mPFC and further evaluated with AAV-Clec2d knocking-down, DNase I, and activated protein C (APC) pretreatment. Moreover, the rescue effect by AAV-Clec2d knocking-down was observed in mice with chronic stress. Mice with chronic stress were presented as obviously depressive- and anxiety-like behaviors and accompanied with significant microglial oxidative stress and inflammation, indicating by reactive oxygen species (ROS) production, primed nuclear factor- $\kappa$ B (NF- $\kappa$ B) signaling pathway, activated NACHT, LRR, and PYD domain-containing protein 3 (NLRP3) inflammasome, and upregulated Clec2d and TLR9 in mPFC, together with histones dictation in cerebrospinal fluid and extracellular trap formation. Stereotactic injection of nucleosomes was contributed to promote microglial inflammation rather than histones in mPFC, indicating that the pro-inflammatory role was derived from extracellular histones-bound DNA but not freely histones. AAV-Clec2d knocking-down, DNase I, and APC were all effective to inhibit nucleosome-induced microglial oxidative stress and inflammation. Moreover, AAV-Clec2d knocking-down in mice with chronic stress exhibited reduced microglial inflammation and improved negative emotional behaviors. Our findings reveal a novel mechanism of DAMP-

associated inflammation that extracellular nucleosomes accelerate microglial inflammation *via* Clec2d and TLR9, and then contribute to chronic stress-induced emotional disorders.

**Keywords:** extracellular nucleosomes, microglia, C-type lectin receptor 2D, toll-like receptor 9, inflammation, chronic stress

## INTRODUCTION

There is a growing body of evidence confirming the bidirectional association between amplified neuroinflammation and chronic stress-related emotional disorders (1, 2). Microglia, a dynamic and active participant in the central nervous system (CNS), play a critical role in maintaining brain homeostasis and surveil the specialized niche of the brain parenchyma for disruptions in homeostasis (3). As an exclusive resident immune-competent cell in the CNS, microglia are capable of secreting an array of pro- and anti-inflammatory cytokines under physiological conditions, such as chronic stress (3, 4). Activated microglia extensively participate in removing cellular debris and apoptotic or necrotic cells by phagocytosis, lending trophic support to neurons and modulating neuronal activity, as well as modifying synaptic connections and plasticity (5). However, previous clinical studies revealed that the overactivated microglia with production of pro-inflammatory cytokines such as tumor necrosis factor- $\alpha$ , interleukin (IL)-1 $\beta$ , and IL-6, are closely associated with the occurrence and severity in patients with neuropsychiatric disorder (6–8). Therefore, microglia have been considered as the dominant mediator, which aggravates and propagates neuroinflammation, contributing to the development of chronic stress-related emotional disorders. An interesting line of evidence suggests that damage-associated molecular patterns (DAMPs) released from damaged and necrotic cell were contributed to the neuroinflammatory process *via* Toll-like receptors (TLRs) (9, 10). However, the origination of neuroinflammation during chronic stress is still remained uncertain (11).

Nucleosome, a repeating structural unit of chromatin that contains histones and DNA, is the basic unit for higher-order chromatin structure and acts as specialized transcription factory in the nucleus. All nucleosome components, including freely histones, DNA, and histones-bound DNA, will be released into the extracellular space during cellular stress and necrosis (12, 13). Extracellular freely histones and DNA are the major DAMPs that induce cytotoxicity and pro-inflammatory signaling through TLR2 and TLR4, as well as TLR9 and intracellular nucleic acid sensing mechanisms, respectively (14). More recently, C-type lectin receptor 2D (Clec2d) has been demonstrated as a dedicated receptor for histones by recognizing sulfated polysaccharides through their basic N-terminal region, providing a novel fascinating avenue for cellular stress and tissue damage sensing pathway (15, 16). However, the pro-inflammatory signaling induced by extracellular nucleosomes has not been studied as extensively as the separate effects brought about by freely histones and DNA, especially in microglia-derived inflammation during chronic stress. Therefore, we designed the present study to investigate the pro-inflammatory

role and mechanism of extracellular nucleosomes and histones to microglia in mice with chronic stress. Additionally, the potential effect of microglia-derived inflammation on spine pruning was discussed.

## METHODS AND MATERIALS

### Animals

Adult male C57BL/6 mice, aged 6–8 weeks, weighted 18–22 g, were housed in the core animal facility with ambient temperature of 22°C  $\pm$  1°C, 30–70% humidity, 12-h dark/12-h light cycle (light on at 07:00 a.m.), and food and water *ad libitum* in Xiamen University. Experimental protocol and all procedures were received prior approval from the Institutional Animal Care and Use Committee at Xiamen University (Xiamen, China, XMULAC20190054). Efforts were made to minimize animal suffering and to reduce the number of animals used.

### Chronic Stress Protocol

Mice were randomly assigned to receive chronic unpredictable mild stress (CUMS), corticosterone (CORT) drinking, or control group. CUMS protocol was involved a variety of mild stressors, including 24 h of food deprivation, 24 h of water deprivation, 1 h of exposure to empty bottles, 8 h of cage tilt (30°), overnight illumination, 24 h of habitation in a soiled cage (200 ml of water in 100 g of sawdust bedding), 5 min of forced swimming (FS) at 8°C, 2 h of physical restraint, and 24 h of exposure to a foreign object (e.g., a piece of plastic) (17). Mice in CUMS group were daily received two of those stressors combination that were prior randomly scheduled for a 4-week period. Mice in CORT group were received CORT drinking water daily for a 6-week period. CORT (Sigma-Aldrich, St. Louis, MO, USA) was dissolved in ethanol absolute (Sigma-Aldrich) and mixed with potable water at a final concentration of 0.1 mg/ml CORT and 1% ethanol (18). Mice in control group were kept without any stress application in the same housing conditions.

### Adeno-Associated Virus Vectors and Stereotaxic Injection

Mice received inhaled anesthesia with 2% isoflurane (RWD Life Science Co., LTD, Shenzhen, China) and positioned in a stereotaxic instrument (RWD Life Science Co., LTD). For knocking-down Clec2d in medial prefrontal cortex (mPFC), pAAV9-U6-mCherry-Clec2d-Mus-593 (titer:  $4.25 \times 10^{12}$ , 5'→3': GGATCAGCAGTACCAGGATCT; GenePharma Co., Ltd, Shanghai, China), or negative control virus pAAV9-U6-mCherry (titer:  $1.04 \times 10^{13}$ , 5'→3': TTCTCCGAACGTGTCA CGT; GenePharma Co., Ltd) was injected into mPFC (AP, +1.70

mm; ML,  $\pm$  0.30 mm; DV,  $-2.80$  mm; 600 nl for each hemisphere) by using a syringe (Hamilton Bonaduz AG, Switzerland) with micropipette (tip diameter,  $\sim 15$   $\mu$ m) attached to a KDS LEGATO 130 micropipette puller (RWD Life Science Co., LTD) at a flow rate of 0.1  $\mu$ l/min followed by an additional 5 min to allow diffusion of the virus. Then, a standard single cannula (RWD Life Science Co., LTD) was bilaterally implanted in mPFC. Mice were housed for 3 weeks for recovery after adeno-associated virus (AAV) injection.

### Intracranial Microinjection

Recombinant nucleosomes (500 nl, 10  $\mu$ g/ml; EpiCypher) or histones (500 nl, 5  $\mu$ g/ml; New England BioLabs, Ipswich, MA, USA) were bilaterally delivered through implanted cannula, and then sacrificed for flow cytometry and fluorescence activated cell sorting (FACS) at the given time points. Recombinant nucleosomes and histones were diluted in artificial cerebrospinal fluid (ACSF) containing 150 mM NaCl, 10 mM D-glucose, 10 mM HEPES, 2.5 mM KCl, 1 mM MgCl<sub>2</sub> (pH 7.35), 312 mOsm. For some experiments, nucleosomes were pretreated with DNase I (100 U; Sigma-Aldrich) to remove DNA or with activated protein C (APC; 100 nM; TopScience Co. Ltd., Shanghai, China) to cleave histones at 37°C for 1 h before intracranial microinjection.

### Open-Field Test

Mice were placed at the center of a cubic arena [50 cm (L)  $\times$  50 cm (W)  $\times$  40 cm (H)]. The free locomotion of mice traveled in 10 min was automatically monitored, recorded, and analyzed by Noldus EthoVision XT (Noldus Information Technology, Wageningen, Netherlands). The total distance and the percentage of time spent in the center area (center time% = center time/total time  $\times$  100%) were calculated.

### Elevated Plus Maze Test

Mice were placed at the center of a plus maze facing one of an open arm. The elevated plus maze (EPM) apparatus consisted of two opposing open arms [50 cm (L)  $\times$  10 cm (W)] and two opposing closed arms with roofless black walls (40-cm height with 60 cm elevated above the floor). The free locomotion of mice traveled in 10 min was automatically monitored, recorded, and analyzed by Noldus EthoVision XT (Noldus Information Technology). The percentage of time spent in the open arms [open arms time% = open arms time/(open arms time + closed arms time)  $\times$  100%] and the percentage of number of entries in the open arms [open arms entries % = open arms entries/(open arms entries + closed arms entries)  $\times$  100%] were calculated.

### Novel Object Recognition Test

Novel object recognition (NOR) test were consisted by habituation, training, and test section with a 60-min separated delay. Briefly, mice were placed at the center of a cubic arena [50 cm (L)  $\times$  50 cm (W)  $\times$  40 cm (H)] without any objects for habituation for 5 min. In the training session, two identical square woodblocks [2 cm (L)  $\times$  2 cm (W)  $\times$  2 cm (H)] were placed in opposite corners of the arena with enough space for mice to move past the woodblocks without interacting with

them. In the test session, mice were presented with one identical woodblock (the familiar object) and another triangle woodblock [2 cm (L)  $\times$  1 cm (W)  $\times$  2 cm (H)] (the novel object). The investigations of mice sniffing and rearing on each object in 5 min were automatically monitored, recorded, and analyzed by Noldus EthoVision XT (Noldus Information Technology). The recognition index including the percentage of time spent with the novel object [recognition index (time) = time spent exploring novel object/time spent exploring both objects] and number of investigations [recognition index (investigations) = number of investigations for exploring novel object/number of investigations for exploring both objects] for exploring the novel object was calculated.

### Sucrose Preference Test

Mice were exposed to sterile water in two identical bottle on the training day 1 and to 1% sucrose (Sigma-Aldrich) solution on the training day 2. The location of two bottles was switched every 12 h to avoid location preference. In the test session, mice were exposed to one bottle of sterile water and the other identical bottle of 1% sucrose solution after 12-h water deprivation. The water and sucrose consumption for 24 h was recorded and the sucrose preference (SP) [SP (%) = sucrose consumption/(sucrose consumption + water consumption)  $\times$  100%] was calculated.

### Tail Suspension Test

Mice tails that were suspended to an acrylic bar (15-cm length with 30 cm elevated above the floor) in 6 min were automatically monitored, recorded, and analyzed by Noldus EthoVision XT (Noldus Information Technology). The immobility time in the last 5-min suspension period was recorded. The percentage of immobility time [immobility time% = immobility time/total time  $\times$  100%] was calculated.

### FS Test

Mice that were placed in a transparent cylindrical container (25-cm height with a diameter of 10 cm) filled with warm water (23°C $\sim$ 25°C) in 6 min were automatically monitored, recorded, and analyzed by Noldus EthoVision XT (Noldus Information Technology). The immobility time (floating behavior) in the last 5-min period was recorded. The percentage of immobility time [immobility time% = immobility time/total time  $\times$  100%] was calculated.

### Immunofluorescence Staining

Mice were deeply anesthetized with inhaling isoflurane (RWD Life Science Co., LTD) and perfused with 50 ml of 0.9% saline followed by 100 ml of 4% paraformaldehyde. Brain was removed and post-fixed in the same fixative overnight and then dehydrated for 48 h at 4°C in 30% sucrose solution. After being embedded with mounting medium (OCT, Tissue-Tek, Sakura, Torrance, CA, USA), transverse frozen sections (50- $\mu$ m thick) were cut by using cryostat (CM1800; Leica, Heidelberg, Germany) and collected serially. The sections were rinsed in 0.01 M phosphate-buffered saline (PBS; pH 7.2 $\sim$ 7.4) three times (10 min each) and blocked with 10% fetal bovine serum (FBS) in 0.01 M PBS containing 0.3% Triton X-100 for

30 min at room temperature (RT). And then, the sections were incubated 4 h at RT and then overnight at 4°C with rabbit anti-Iba-1 antibody (1:200; Abcam) and rat anti-CD68 antibody (1:200; Santa Cruz Biotechnology, Santa Cruz, CA, USA) or goat anti-Clec2d antibody (1:200; Abcam) and rabbit-anti-Eea1 (1:200; Abcam), rabbit-anti-Rab7 (1:200; Abcam), or rabbit-anticlreticulin (1:200; Abcam). The sections were washed three times with 0.01 M PBS (10 min each) and then incubated for 2 h at RT with Alexa Fluor 488 donkey anti-rabbit or Alexa Fluor 488 donkey anti-goat and Alexa Fluor 594 donkey anti-rat immunoglobulin G (1:1000; Abcam). Finally, the sections were mounted with mounting medium containing 4',6-diamidino-2-phenylindole (DAPI) (Abcam) after washing three times with 0.01 M PBS (10 min each) as well as obtained and three-dimensional reconstructed by using a confocal laser scan microscope (Zeiss LSM 980 Airyscan; Carl Zeiss Microscopy GmbH, Promenade, Jena, Germany).

## Flow Cytometry and FACS

Mice were sacrificed under deep anesthesia with inhaling isoflurane (RWD Life Science Co., LTD) and the brains were quickly removed in filtered FACS buffer containing 0.01 M PBS with 0.5% FBS on ice. Meninges, blood vessels, and choroid plexus were carefully separated and then bilateral mPFC was finely minced prior to digestion. Chopped mPFC was placed in glass homogenizer with a total volume of 1 ml of FACS buffer containing DNase I (20 U; Sigma-Aldrich), papain (20 U; Sigma-Aldrich), and dispase II (1.2 U; Sigma-Aldrich), and then processed with a mechanic dissociator at 6 rpm for 30 min at RT. Prior to use, papain was activated for 30 min at 37°C and 5% CO<sub>2</sub>. To stop all digestions, samples were diluted with cold FACS buffer and placed on ice. Solutions were then further homogenated and filtered through a 70-µm cell strainer (BD Biosciences, NJ, USA). The resulting single-cell suspension was centrifuged at 300g for 10 min at RT. Percoll (GE Healthcare, USA) gradient was used to remove myelin and enrich the homogenate for viable microglial cells. A stock solution of isotonic Percoll was prepared (9:1 Percoll in 0.1 M PBS). Cell pellets were resuspended in a 30% stock isotonic Percoll (SIP) diluted with HyClone Dulbecco's modified Eagle's medium (Gibco, Thermo Fisher Scientific, Waltham, MA, USA). Gradient were centrifuged without brake for at 300g for 30 min at RT. After centrifugation, cells were collected and washed with cold FACS buffer, centrifugated for 10 min at 300g, and resuspended and incubated in 0.5 ml of 1× red blood cell lysis buffer (Solarbio Life Science) at RT for 5 min. Solutions were centrifuged at 300g for 10 min and cells were finally resuspended in 100 µl of FACS buffer on ice before flow cytometry staining. Fc receptor blocking reagent for mouse (1:100; BioLegend, USA) was added to the FACS buffer containing the cell suspension to block surface antigens in microglial cells or macrophages and incubated for 10 min. For surface staining, rabbit anti-Clec2d antibody (1:200; Abcam) was incubated for 30 min, washed with cold FACS buffer, and centrifugated for 10 min at 300g; then, a mixture containing fluorochrome-conjugated antibodies recognizing mouse CD45-PE, CD11b-FITC, I-A/I-E-BV421 (1:200; BD Biosciences), and Alexa Fluor 594 donkey anti-

rabbit (1:1000; Abcam) was incubated for another 30 min. Samples were washed with 500 µl of FACS buffer and centrifugated for 10 min at 300g in each step. For intracellular staining, samples were incubated with 250 µl of 1 × fixation/permeabilization solution (BD Biosciences) for 20 min at RT after surface staining. And then, samples were washed with 500 µl of 1 × BD Perm/Wash™ buffer (BD Biosciences) and centrifugated for 10 min at 300g. Cells were resuspended with rabbit anti-Clec2d antibody (1:200; Abcam), incubated for 30 min, washed with cold FACS buffer, centrifugated for 10 min at 300g, and then incubated with Alexa Fluor 594 donkey anti-rabbit (1:1000; Abcam) for another 30 min. For ROS incubation, cell pellets were incubated with 2',7'-Dichlorodihydrofluorescein diacetate (DCFH-DA) (1:1000; Beyotime Biotechnology, Shanghai, China) for 20 min at 37°C and 5% CO<sub>2</sub> before surface staining. Finally, cell pellets were resuspended in 250 µl of FACS buffer and samples were immediately used for flow cytometry by using Beckman Cytoflex LX (Beckman Coulter, Inc., CA, USA) or FACS by using MoFlo Astrios EQS Cell Sorter (Beckman Coulter, Inc.).

## Western Blotting

CD11b<sup>+</sup>CD45<sup>Low</sup> microglia were collected by FACS with a number of 1 × 10<sup>5</sup>. Cell pellets were lysed with 2× loading buffer with proteinase and phosphatase inhibitor cocktail (Solarbio Life Science). The electrophoresis samples were heated at 100°C for 10 min and loaded onto 10% SDS-polyacrylamide gels with standard Laemmli solutions (Bio-Rad Laboratories, CA, USA). After the proteins were electroblotted onto a polyvinylidene difluoride membrane (Immobilon-P, Millipore, Billerica, MA, USA), the membranes were placed in a blocking solution containing tris-buffered saline with 0.02% Tween 20 (TBS-T; Sigma-Aldrich) and 5% non-fat dry milk (Sigma-Aldrich) and incubated for 60 min under gentle agitation at RT, then at 4°C for overnight with goat anti-Clec2d antibody (1:1000; Abcam), rabbit anti-TLR9 antibody (1:1000; Abcam), rabbit anti-citH3 antibody (1:1000; Abcam), goat anti-citrullinating enzyme peptidylarginine deiminase type 4 (PAD4) antibody (1:1000; Abcam), rabbit anti-nuclear factor-κB (NF-κB) p65 antibody (1:1000; Cell Signaling Technology Inc.), rabbit anti-p-NF-κB p65 antibody (1:1000; Cell Signaling Technology Inc.), rabbit anti-inhibitor of NF-κB α (IκBα) antibody (1:1000; Cell Signaling Technology Inc.), rabbit anti-p-IκBα antibody (1:1000; Cell Signaling Technology Inc.), rabbit anti-NOD-like receptors (NLRs) family pyrin domain-containing 3 (NLRP3) antibody (1:1000; Cell Signaling Technology Inc.), rabbit anti-cleaved caspase-1 antibody (1:1000; Cell Signaling Technology Inc.), rabbit anti-IL-1β antibody (1:1000; Cell Signaling Technology, Inc.), rabbit anti-cleaved IL-1β antibody (1:1000; Cell Signaling Technology, Inc.), or mouse anti-β-actin antibody (1:5000; Sigma-Aldrich). Bound primary antibodies were detected by incubating with anti-mouse, anti-rabbit, or anti-goat horseradish peroxidase-conjugated secondary antibody (1:10000; Amersham Pharmacia Biotech Inc., Piscataway, NJ, USA) for 2 h under gentle agitation at RT. Between each step, the immunoblots were rinsed with TBS-T three times (10 min each). Protein blots' densities were detected by using enhanced chemiluminescence (Solarbio Life Science)

and analyzed in the Bio-Rad ChemiDoc Imaging System (Bio-Rad Laboratories Ltd, USA). Immunoreactive bands were quantified and normalized to  $\beta$ -actin.

## Enzyme Linked Immunosorbent Assay

CORT, IL-1 $\beta$ , and extracellular nucleosomes levels were measured by using enzyme linked immunosorbent assay (ELISA) kits for CORT (Cloud Clone Crop., Wuhan, China), IL-1 $\beta$  (Cloud Clone Crop.), or nucleosomes (Cell Death Detection ELISA<sup>PLUS</sup>, Roche, Hvidovre, Denmark) according to the instructions.

## Statistical Analysis

Data were expressed as mean  $\pm$  standard error of the mean (SEM) unless otherwise specified. Paired or independent Student's *t*-test was used for two groups comparison and two- or three-way or repeated measurement analysis of variance (ANOVA) followed by Tukey's *post hoc* test was used for multiple comparison as appropriate. The area under the time-course curves values during the analysis time was used to measure the summed effects of body weight. The linear regression was conducted to analyze the correlation between nucleosomes in CSF and IL-1 $\beta$  in mPFC. Sholl analysis was applied to analyze microglial morphology by counting the number and length of branch tips with ImageJ (<http://imagej.net>). All these data were analyzed by using GraphPad Prism version 8.3.0 for Windows (Graph Pad Software, San Diego California USA, [www.graphpad.com](http://www.graphpad.com)).  $P < 0.05$  was considered as statistical significance.

## RESULTS

### Mice With Chronic Stress Exhibited Negative Effects on Daily Weight Gain and Emotional Behaviors

Mice with chronic stress were experienced CUMS and CORT drinking for 4 weeks (**Figure 1A**). Compared with CONT group, mice in CUMS and CORT groups showed substantially boosted serum CORT ( $P < 0.001$ ; **Figure 1B**), indicating a stressful condition of mice during chronic stress. Besides, mice in CUMS and CORT groups also presented negative effects on daily weight gain, compared with CONT group, indicated by significantly reduced body weight ( $P < 0.001$ ; **Figure 1C**) and daily food intake ( $P < 0.001$ ; **Figure 1D**).

Chronic stress was associated with negative emotional behaviors. Compared with CONT group, mice in CUMS and CORT groups presented a significantly decreased center time% ( $P < 0.001$ ) with similar total distance in open-field (OF) test ( $P > 0.05$ ; **Figure 2A**), as well as a reduced OA time% ( $P < 0.001$ ) and open arms (OA) entries% in EPM test ( $P < 0.05$ ; **Figure 2B**), indicating the anxiety-like emotion without locomotion impairment. Compared with CONT group, mice in CUMS and CORT groups presented a significantly decreased recognition index on novel object investigations and time in NOR test ( $P < 0.001$ ; **Figure 2C**), indicating the cognitive dysfunction.

Compared with CONT group, mice in CUMS and CORT groups presented a significantly decreased SP in SP test ( $P < 0.001$ ; **Figure 2D**), as well as a prolonged immobility time% in both FS ( $P < 0.001$ ; **Figure 2E**) and tail suspension (TS) tests ( $P < 0.001$ ; **Figure 2F**), indicating the depression-like emotion.

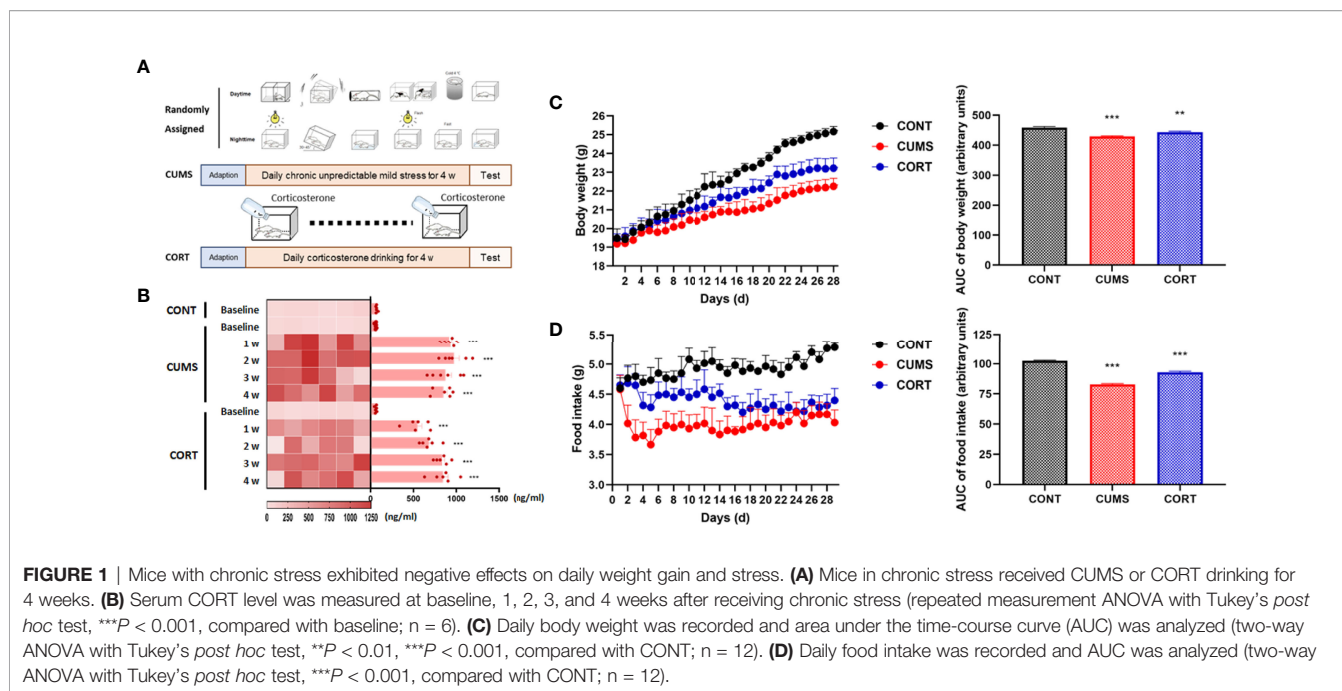
### Extracellular Nucleosomes Were Dictated in mPFC of Mice With Chronic Stress

Chronic stress induces cell death and necrotic cells release DAMPs and triggered neuroinflammation (19, 20). Intracellular histones release predominantly depends on posttranscriptional modification that histones citrullination mediated by their encoding PAD4 (21). Our findings suggested that the expression of citrullinated histones H3 and PAD4 was significantly increased ( $P < 0.01$ ; **Figures 3A,G**) and showed colocalization (**Figure 3C**). Moreover, citH3<sup>+</sup> neurons showed a close relationship with microglia (**Figure 3B**) in mPFC in CUMS and CORT groups, compared with CONT group. We further confirmed extracellular histones (**Figure 3D**) and extracellular nucleosomes in CSF in CUMS and CORT groups ( $P < 0.05$ , **Figure 3E**). Importantly, positive correlations were found in nucleosome in CSF and IL-1 $\beta$  in mPFC in CUMS and CORT group with  $r^2 = 0.8957$  and  $0.8234$ , respectively (**Figure 3F**).

### Mice With Chronic Stress Were Accompanied With Microglial Activation and Inflammation in mPFC

Increasing evidence has suggested that neuroinflammation is contributed to emotional disorders induced by chronic stress, and microglia play the executive role of immunity and inflammation in CNS. Therefore, we primarily focused on microglial biological function during chronic stress. Our morphological results and Sholl analysis showed that microglial pro-inflammatory activation in CUMS and CORT groups was indicated by proliferated microglia ( $P < 0.001$ ; **Figure 4A**) with increased soma volume and retracted processes ( $P < 0.001$ ; **Figure 4B**). Moreover, we investigated CD68 expression, a classic phagocytic marker for activated monocytes and macrophages, in microglia. The results indicated that increased CD68 expression was observed in mPFC of mice with CUMS and CORT, compared with CONT group ( $P < 0.001$ ; **Figure 4C**), indicating a pro-phagocytic activation state of microglia in mPFC. Since microglial inflammation was associated with neuronal synaptic plasticity, we additionally confirmed the significantly decreased density of spine, specifically for mushroom type, in mPFC of mice with CUMS and CORT, compared with CONT group by using sparse labeling technique (**Supplementary Figure 1**).

For specifically identifying more the change of microglia during chronic stress, we further investigated by using flow cytometry and cell sorting (**Figure 5A**). Microglia in mPFC were harvested and Western blot was performed. The results from CD11b<sup>+</sup>CD45<sup>low</sup>MHC-II<sup>+</sup> microglia in mPFC (**Figure 5B**) showed that a significant higher level of cerebral IL-1 $\beta$  ( $P < 0.001$ , **Figure 5C**) and a proportion of activated microglia ( $P < 0.001$ , **Figure 5D**) with increased ROS production (**Figure 5E**).



were shown in CUMS and CORT groups, compared with CONT group. Moreover, the Western blot data also conformed the primed NF- $\kappa$ B signaling pathway indicated by upregulated p-p65, p-I $\kappa$ B $\alpha$ , pro-caspase 1, and pro-IL-1 $\beta$ , as well activated NLRP3 inflammasome indicated by upregulated NLRP3, ASC, cleaved-caspase 1, and cleaved IL-1 $\beta$ , in CUMS and CORT groups, compared with CONT group ( $P < 0.05$ ; **Figure 5H**). Besides, microglial Clec2d, a newly defined cellular death sensor, and TLR9, a classic intracellular DNA sensor, were also found to be increased in CUMS and CORT groups, compared with CONT group (**Figures 5F-H**).

## Extracellular Nucleosomes Accelerated Microglial Oxidative Stress and Pro-Inflammatory Activation But Not Histones in mPFC

For specifically identifying the pro-inflammatory role and mechanism of extracellular nucleosomes and histones, stereotactic injection of recombinant nucleosomes and histones was conducted in mPFC *in vivo*. Previous studies indicated that injection of 1.25 mg of purified histones was lethal within 1 h, and serum levels of histones as high as 3 ng/ml presented coagulopathy, endothelial damage, and organ dysfunction in human (22, 23). Moreover, a concentration of 500  $\mu$ g/ml of externalized histones H4 orchestrated chronic inflammation by inducing lytic smooth muscle cells death and 200 nM extracellular histones H1 exhibited significant neurotoxicity (24, 25). However, whether extracellular nucleosomes exhibited cytotoxic effects remained controversial. Some studies reported that isolated nucleosomes do not induce cell death of cultured endothelial cells *in vitro* (26, 27). Nonetheless, some have described that nucleosomes induced necrotic cell death

specifically in cultured lymphocytes and *in vivo* in a dose- and time-dependent manner (28). Thus, we investigated the concentration-dependent promicroglial death and promicroglial activation profile for recombinant nucleosomes and histones prior to *in vivo* study. The results showed a concentration of more than 10  $\mu$ g/ml histones of the presented significant neurotoxicity for primary neuron, but not for nucleosomes, even at a relatively high concentration of 15  $\mu$ g/ml (**Supplementary Figure 2**). Considering that cytotoxicity triggers chronic inflammation and microglial activation secondary to cell death, we performed bilateral stereotactic injection of 10  $\mu$ g/ml of recombinant nucleosomes and 5  $\mu$ g/ml histones in mPFC in a volume of 1  $\mu$ l. Interestingly, nucleosomes induced significantly microglial oxidative stress and pro-inflammatory activation indicated by more ROS production, upregulated of major histocompatibility complex II (MHC-II) expression, and IL-1 $\beta$  secretion in a time-dependent manner, while the pro-inflammatory profile was limited for histones injection ( $P < 0.001$ , **Figures 6A, D-F**).

## Extracellular Nucleosomes Accelerated Microglial Inflammation via Clec2d and TLR9

Considering that the microglial inflammation reached the peak on 3 days after stereotactic injection, we further investigated Clec2d and TLR9 expression on 3 days after stereotactic injection. The results revealed that Clec2d on the member and intracellular was significantly increased, while the significant increase of TLR9 was shown in nucleosomes injection, instead of histones (**Figures 6B, C**). Furthermore, the results of Clec2d intracellular expression showed that Clec2d was colocalized with late endosome (indicated by colocalization of Clec2d and Rab7)

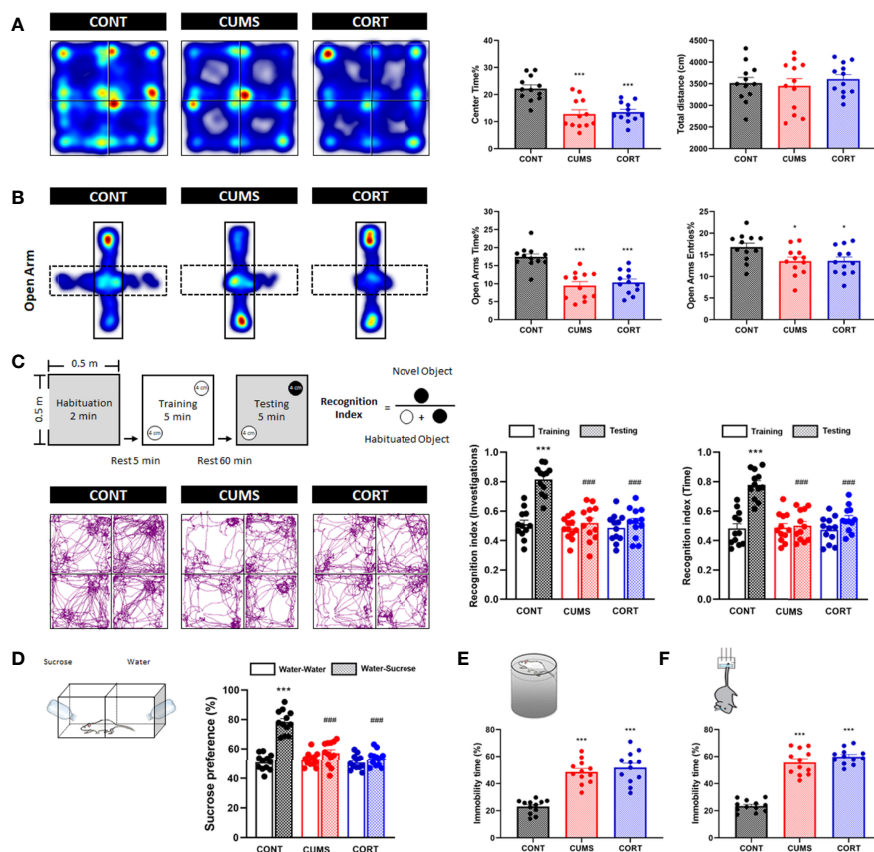


**FIGURE 2** | Mice with chronic stress exhibited negative emotional behaviors. **(A)** Representative heat maps for CONT, CUMS, and CORT groups in OF test were presented, and center time% and total distance were analyzed (two-way ANOVA with Tukey's *post hoc* test,  $***P < 0.001$ , compared with CONT;  $n = 12$ ).

**(B)** Representative heat maps for CONT, CUMS, and CORT groups in EPM test were presented, and open arm time% and open arm entries% were analyzed (two-way ANOVA with Tukey's *post hoc* test,  $*P < 0.05$ ,  $***P < 0.001$ , compared with CONT;  $n = 12$ ). **(C)** Experimental protocol and representative trajectory images for CONT, CUMS, and CORT groups in NOR test were presented, and recognition index of investigations and time was analyzed (paired Student's *t*-test,  $***P < 0.001$ , compared with training. Two-way ANOVA with Tukey's *post hoc* test,  $###P < 0.001$ , compared with CONT-testing;  $n = 12$ ). **(D)** Experimental protocol for SP test was presented, and sucrose preference was analyzed (paired Student's *t*-test,  $***P < 0.001$ , compared with water-water. Two-way ANOVA with Tukey's *post hoc* test,  $###P < 0.001$ , compared with CONT-water-sucrose;  $n = 12$ ). **(E)** Experimental protocol for FS test was presented, and immobility time% was analyzed (two-way ANOVA with Tukey's *post hoc* test,  $***P < 0.001$ , compared with CONT;  $n = 12$ ). **(F)** Experimental protocol for TS test was presented, and immobility time% was analyzed (Two-way ANOVA with Tukey's *post hoc* test,  $***P < 0.001$ , compared with CONT;  $n = 12$ ).

and endoplasmic reticulum (indicated by colocalization of Clec2d and calreticulin), instead of early endosome (**Figure 7A**). Together with the results that significant increase of intracellular Clec2d, this might indicate an internalization of Clec2d with nucleosomes and histones stimulation. Considering the absence of enlarged microglial inflammation in histones injection, we further investigated microglia intracellular pro-inflammatory signaling pathway in mPFC on 3 days after nucleosomes and histones stereotactic injection with or without Clec2d knocking-down, respectively. Compared with histones stereotactic injection, nucleosomes significantly upregulated TLR9, Myd88, and p-p65 expression, while, previously, local knocking-down of Clec2d by AAV-Clec2d obviously eliminated the activation of TLR9-NF- $\kappa$ B signaling pathway ( $P < 0.01$ , **Figure 7B**). However, no significant activation of the other mitogen-activated protein kinase

(MAPK) pathways, including p-ERK, p-p38, and p-Jnk, was detected (**Supplementary Figure 3**). Considering the previous study has revealed that Clec2d was not a signaling receptor, and together with the fact that stimulation of Clec2d with histones did not induce cytokine responses (16), we further investigated the Syk signaling pathway, the knowing downstream signaling kinase of activating C-type lectin receptors (CLRs). The results showed no obvious detectable Clec2d-dependent activation of Syk with nucleosomes and histones stimulation ( $P > 0.05$ , **Figure 7B**). Importantly, knocking-down of Clec2d by AAV-Clec2d inhibited microglial oxidative stress, pro-inflammatory activation, and cytokine production induced by extracellular nucleosomes ( $P < 0.001$ , **Figures 7C-E**). Moreover, the ability of extracellular nucleosomes to stimulate ROS production, MHC-II expression, and IL-1 $\beta$  secretion in microglia would be abolished when it was pretreated with DNase I to remove DNA

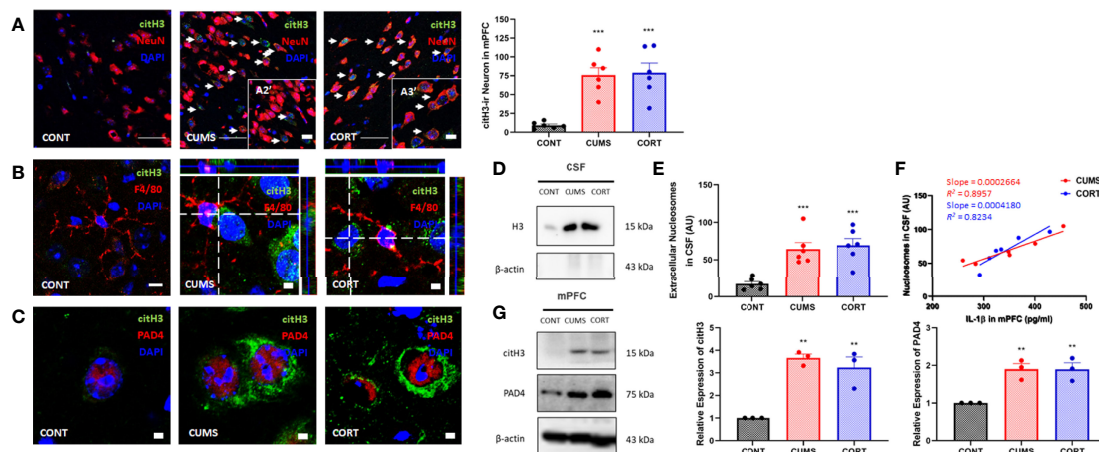


**FIGURE 3** | Chronic stress induced extracellular histones release and extracellular trap formation in mPFC. **(A)** Representative immunofluorescence images showing the citH3<sup>+</sup> and NeuN<sup>+</sup> in CONT, CUMS, and CORT groups were presented, and citH3-ir neurons in mPFC was analyzed (two-way ANOVA with Tukey's *post hoc* test *post hoc*, \*\*\**P* < 0.001, compared with CONT. Two replica for *n* = 3). Scale bars: 20x and 40x. **(B)** Representative immunofluorescence images showing the relationship of F4/80<sup>+</sup> microglia and citH3<sup>+</sup> cells in CONT, CUMS, and CORT groups were presented. Scale bar: 126x. **(C)** Representative immunofluorescence images showing the relationship of citH3 and PAD4 in CONT, CUMS, and CORT groups were presented. Scale bar: 126x. **(D)** Representative Western blots showing extracellular histone H3 in CSF. **(E)** Concentration of nucleosomes in CSF was analyzed (two-way ANOVA with Tukey's *post hoc* test *post hoc*, \*\*\**P* < 0.001, compared with CONT; *n* = 6). **(F)** Regression analysis between nucleosomes in CSF and IL-1β in mPFC was presented (linear regression; *n* = 6). **(G)** Representative Western blots showing citH3 and PAD4 in mPFC were presented. Relative expression of citH3 and PAD4 was analyzed (two-way ANOVA with Tukey's *post hoc* test *post hoc*, \*\**P* < 0.01, compared with CONT; *n* = 3). *post hoc*.

or APC to cleave histones (*P* < 0.001, **Figures 7F-H**). For further identifying the role of TLR9, we investigated the microglial inflammation induced by recombinant nucleosomes with Clec2d or/combined with TLR9 antagonist E6446

dihydrochloride treatment. The results showed that both Clec2d knocking-down, TLR9 inhibitor, and Clec2d knocking-down combined with TLR9 inhibitor significantly inhibited microglial IL-1β expression. Moreover, Clec2d knocking-down

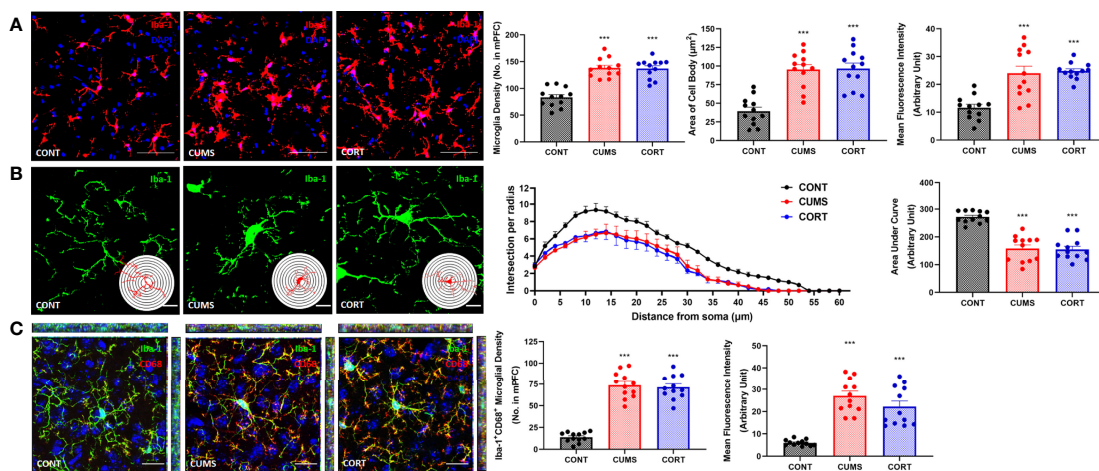
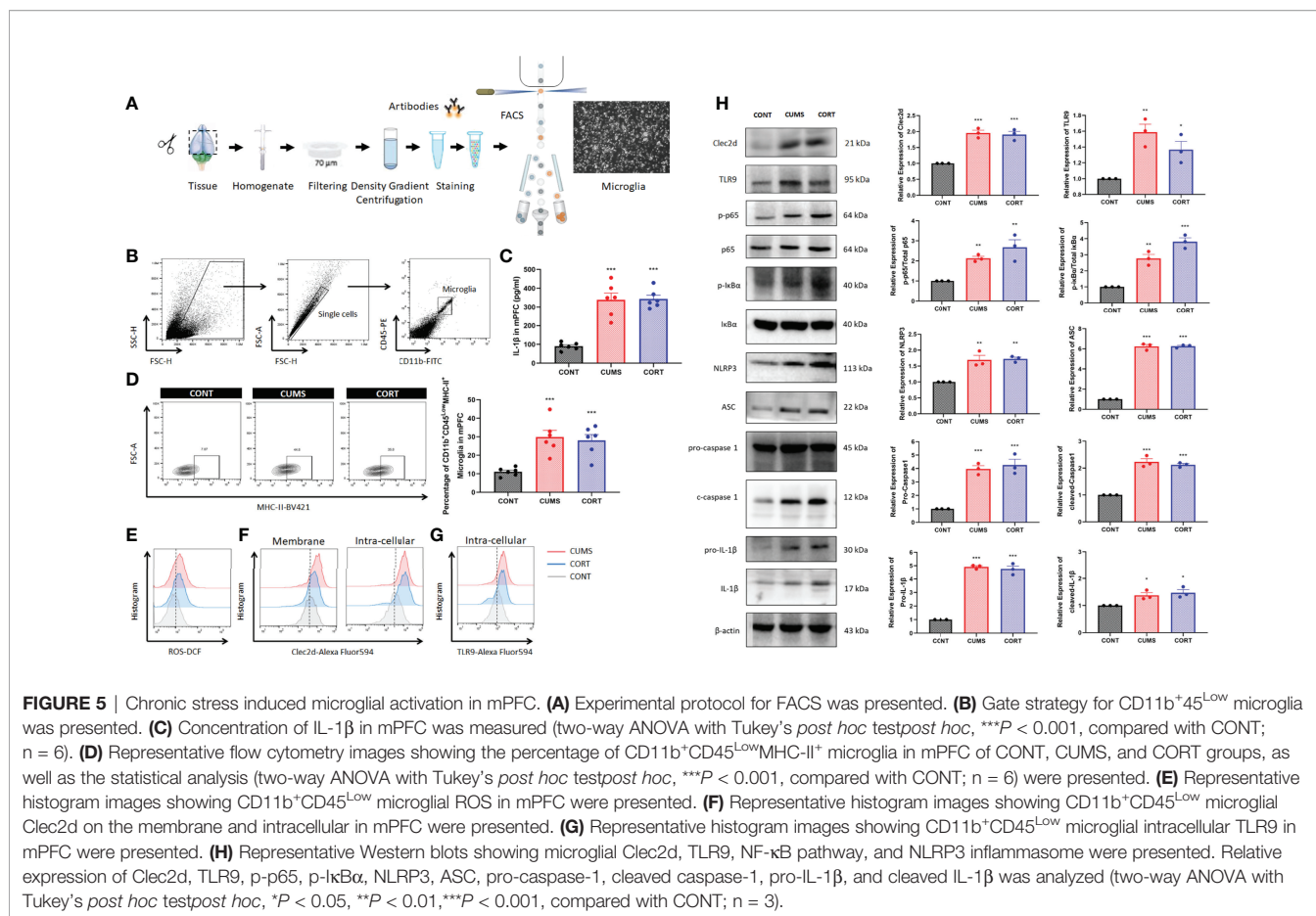


**FIGURE 4** | Mice with chronic stress were accompanied with microglial activation in mPFC. **(A)** Representative immunofluorescence images showing the Iba-1<sup>+</sup> microglia in CONT, CUMS, and CORT groups were presented, and the microglial density, area of cell body, and the MFI of Iba-1 were analyzed (two-way ANOVA with Tukey's *post hoc* test *post hoc*, \*\*\**P* < 0.001, compared with CONT. Two replica for *n* = 6). Scale bar: 40x. **(B)** Representative immunofluorescence images showing the 3D reconstruction of Iba-1<sup>+</sup> microglia in CONT, CUMS, and CORT groups were presented, and Sholl analysis and their AUCs were analyzed (two-way ANOVA with Tukey's *post hoc* test *post hoc*, \*\*\**P* < 0.001, compared with CONT. Two replica for *n* = 6). Scale bar: 126x. **(C)** Representative immunofluorescence images showing the co-localization of CD68<sup>+</sup> and Iba-1<sup>+</sup> microglia in CONT, CUMS, and CORT group were presented, and the Iba-1<sup>+</sup>CD68<sup>+</sup> microglial density and also the MFI of CD68 were analyzed (two-way ANOVA with Tukey's *post hoc* test *post hoc*, \*\*\**P* < 0.001, compared with CONT. Two replica for *n* = 6). Scale bar: 63x.



combined with TLR9 inhibitor was superior to Clec2d knocking-down, while no obvious synergic effect was found when compared with TLR9 alone (**Supplementary Figure 4**). Taken together, our results revealed that the amplified pro-inflammatory mechanism of nucleosomes (histones-bound DNA) might be derived from Clec2d-mediated histones-bound DNA internalization and DNA-mediated endosomal TLR9-dependent activation of NF- $\kappa$ B signaling pathway.

## Clec2d Knocking-Down Reduced Microglial Activation and Inflammation in mPFC As Well As Improved Negative Emotional Behaviors

For further confirming the role of Clec2d-dependent extracellular nucleosomes in mPFC of mice with chronic stress, bilateral stereotactic injection of AAV-Clec2d was performed to knock down Clec2d in mPFC prior to receiving CUMS and CORT drinking (**Figure 8A** and **Supplementary Figure 5**). Our results revealed an obvious decrease of microglial ROS production (**Figure 8B** and **Supplementary Figure 5**), MHC-II expression (*P* < 0.001, **Figure 8C** and **Supplementary Figure 5**), and IL-1 $\beta$  secretion (*P* < 0.001, **Figure 8D** and **Supplementary Figure 5**) in mPFC. Moreover, Clec2d knocking-down also

significantly rescued the decreased density of mushroom type spine in mPFC of mice with CUMS and CORT (**Supplementary Figure 6**). Notably, the negative emotional behaviors were significantly improved indicated by increased center time% in OF (*P* < 0.001, **Figure 8E** and **Supplementary Figure 5**), OA time% and OA entries% in EPM (*P* < 0.01, **Figure 8F** and **Supplementary Figure 5**), recognition index in NOR (*P* < 0.01, **Figure 8G** and **Supplementary Figure 5**), sucrose preference in SP (*P* < 0.001, **Figure 8H** and **Supplementary Figure 5**), and immobility time% in both FS (*P* < 0.001, **Figure 8I** and **Supplementary Figure 5**) and TS (*P* < 0.001, **Figure 8J** and **Supplementary Figure 5**) tests in AAV-Clec2d group, compared with CUMS and AAV-Veh groups.

## DISCUSSION

Here, we reported that mice with chronic stress were presented as significant microglial oxidative stress and inflammation, indicating by ROS production, primed NF- $\kappa$ B signaling pathway, activated NLRP3 inflammasome, and upregulated Clec2d and TLR9 in mPFC, together with mushroom-type spine loss, as well as histones and nucleosomes in CSF dictation. Stereotactic injection of nucleosomes was

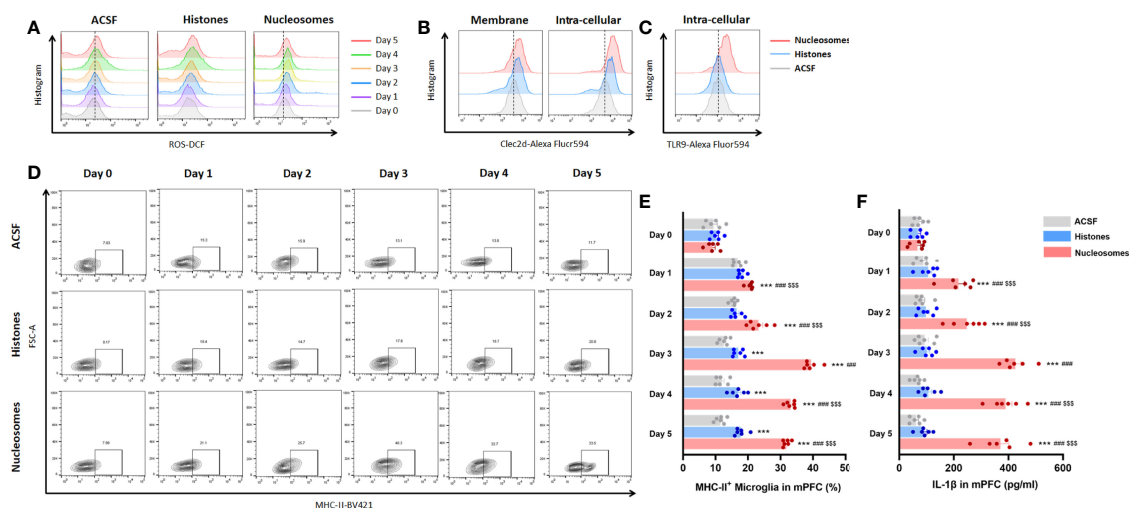


**FIGURE 6** | Extracellular nucleosomes accelerated microglial oxidative stress and pro-inflammatory activation but not histones in mPFC. **(A)** Representative histogram images showing CD11b<sup>+</sup>CD45<sup>LOW</sup> microglial ROS before and 1–5 days after ACSF, histones, and nucleosomes stereotactic injection in mPFC were presented. **(B)** Representative histogram images showing CD11b<sup>+</sup>CD45<sup>LOW</sup> microglial Clec2d on the membrane and intracellular on day 3 after ACSF, histones, and nucleosomes stereotactic injection in mPFC were presented. **(C)** Representative histogram images showing intracellular TLR9 on day 3 after ACSF, histones, and nucleosomes stereotactic injection in mPFC were presented. **(D)** Representative flow cytometry images showing the percentage of CD11b<sup>+</sup>CD45<sup>LOW</sup>MHC-II<sup>+</sup> microglia before and 1–5 days after ACSF, histones, and nucleosomes stereotactic injection in mPFC were presented. **(E)** Percentage of CD11b<sup>+</sup>CD45<sup>LOW</sup>MHC-II<sup>+</sup> microglia before and 1–5 days after ACSF, histones, and nucleosomes stereotactic injection in mPFC was analyzed (repeated measurement ANOVA with Tukey's *post hoc* test,  $***P < 0.001$ , compared with CONT;  $###P < 0.001$ , compared with Histones;  $$$$P < 0.001$ , compared with nucleosomes day 0;  $n = 6$ ). **(F)** Concentration of IL-1 $\beta$  before and 1–5 days after ACSF, histones, and nucleosomes stereotactic injection in mPFC was analyzed (repeated measurement ANOVA with Tukey's *post hoc* test,  $***P < 0.001$ , compared with CONT;  $###P < 0.001$ , compared with histones;  $$$$P < 0.001$ , compared with nucleosomes day 0;  $n = 6$ ).

contributed to promote microglial inflammation rather than cell-free histones in mPFC. AAV-Clec2d knocking-down, pretreatment with DNase I to remove DNA, and APC to cleave histones were all effective to inhibit nucleosomes-induced microglial oxidative stress and inflammation. Moreover, AAV-Clec2d knocking-down in mice with chronic stress exhibited limited microglial inflammation, reduced mushroom type spine loss, and improved negative emotional behaviors. The graphic summary was presented in **Figure 9**.

During the recent decade, a surge of clinical and preclinical findings has implicated neuroinflammation as the etiology of stress-related emotional disorders, including anxiety and depression (29). Fast-evolving human neuroimaging techniques provide a more fine-grained understanding of neuroinflammatory response to stress and make it closer to the reality (30). Some preclinical studies have suggested an elevated microglial-derived neuroinflammation in varied neuropsychiatric disorders by using 18-kDa translocator protein positron emission tomography, which is expressed on activated microglia to quantify central neuroinflammation and has been considered as a promising new validating microglial inflammatory biomarker in psychiatric and neurological disorders (31–33). Mapping studies have identified a cluster of subcortical (basal ganglia, ventral striatum, hippocampus, hypothalamus, and amygdala) and cortical (insula, anterior cingulate, orbitofrontal, ventromedial, and dorsolateral prefrontal cortices) structures that appear central to effects of

neuroinflammation on psychological function linked to psychopathology (34, 35). It is worth noting that a diverse array of human and animal studies has demonstrated that mPFC is a key node of cortical and subcortical networks that is critical for the generation and regulation of negative emotion, through its interactions with amygdala, bed nucleus of stria terminalis, periaqueductal gray, hippocampus, and dorsal anterior cingulate cortex (36). However, providing further insight into “how” rather than simply “where” a particular neuroinflammatory process works within the brain during chronic stress is urgently needed. Therefore, we primarily focused on “how” the microglia initiated and accelerated neuroinflammation in mPFC in present study. Our morphological and flow cytometric findings indicated the pro-inflammatory and pro-phagocytic activation of microglia indicated by increased soma volume, retracted processes, ROS production, and upregulated CD68 and also MHC-II expression (37). Moreover, excessive pro-inflammatory and pro-phagocytic activation of microglia is contributed to spine pruning and synaptic transmission impairment, and then leads to development and progression of emotional disorders (38, 39). Similarly, a firmly line of our findings also showed that significantly decreased density of spine, especially mushroom type, in mPFC of mice with CUMS and CORT was observed. Interestingly, Clec2d knocking-down significantly rescued the decrease of mushroom type spine in mPFC of mice with chronic stress to a large extent.

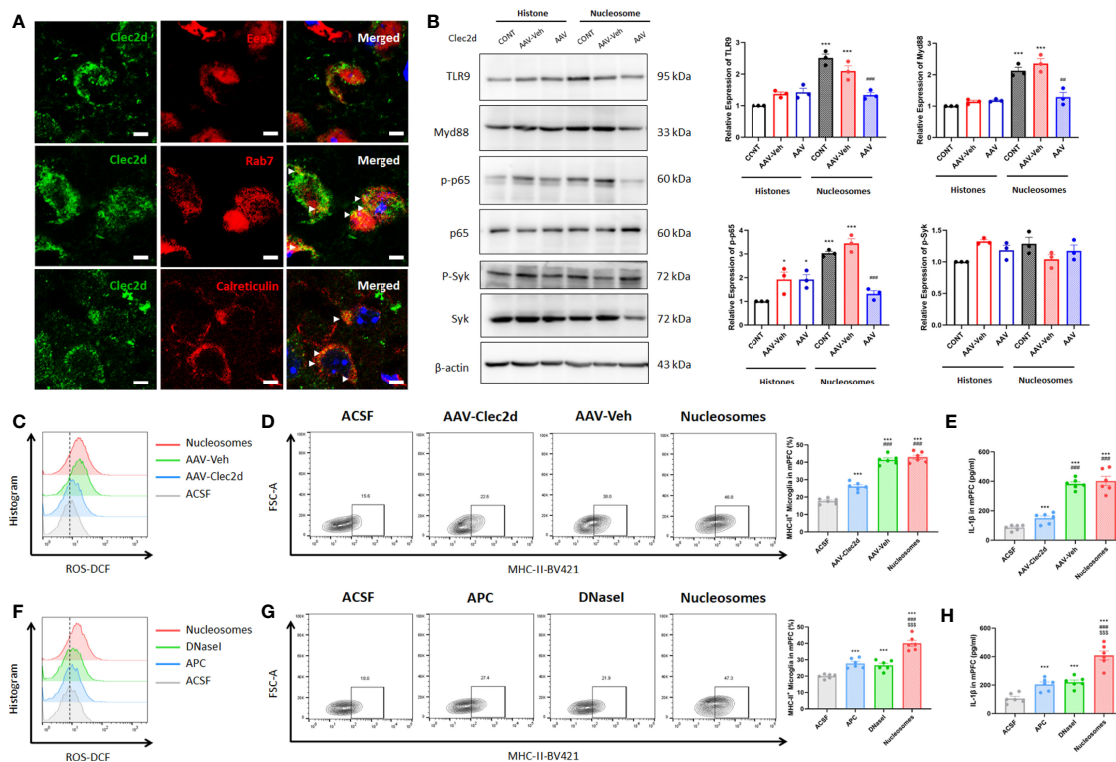


**FIGURE 7** | Extracellular nucleosomes accelerated microglial inflammation via Clec2d and TLR9. **(A)** Representative immunofluorescence images showing the subcellular location of Clec2d and Eea1, Rab7, and calreticulin, as well as their relationship in primary microglia were presented. Scale bar: 150x. **(B)** Representative Western blots showing the expression of microglial TLR9, Myd88, p-p65, and p-Syk on 3 days after ACSF, histones, or nucleosomes stereotactic injection in mPFC with Clec2d knocking-down were presented. Relative expression of TLR9, Myd88, p-p65, and p-Syk on 3 days after ACSF, histones, or nucleosomes stereotactic injection in mPFC with Clec2d knocking-down was analyzed (two-way ANOVA with Tukey's *post hoc test* *post hoc*,  $^*P < 0.05$ ,  $^{***}P < 0.001$ , compared with histones;  $^{\#}P < 0.01$ ,  $^{\#\#}P < 0.001$ , compared with Nucleosomes-AAV-Veh;  $n = 3$ ). **(C)** Representative flow cytometry images showing CD11b<sup>+</sup>CD45<sup>Low</sup> microglial ROS on 3 days after ACSF or nucleosomes stereotactic injection in mPFC with Clec2d knocking-down were presented. **(D)** Representative flow cytometry images and statistical analysis showing the percentage of CD11b<sup>+</sup>CD45<sup>Low</sup>MHC-II<sup>+</sup> microglia on 3 days after ACSF or nucleosomes stereotactic injection in mPFC with Clec2d knocking-down were presented (two-way ANOVA with Tukey's *post hoc test* *post hoc*,  $^{***}P < 0.001$ , compared with ACSF;  $^{\#\#}P < 0.001$ , compared with AAV-Clec2d;  $n = 6$ ). **(E)** Concentration of IL-1 $\beta$  on 3 days after ACSF or nucleosomes stereotactic injection in mPFC with Clec2d knocking-down was analyzed (two-way ANOVA with Tukey's *post hoc test* *post hoc*,  $^{***}P < 0.001$ , compared with ACSF;  $^{\#\#}P < 0.001$ , compared with AAV-Clec2d;  $n = 6$ ). **(F)** Representative flow cytometry images showing CD11b<sup>+</sup>CD45<sup>Low</sup> microglial ROS on 3 days after ACSF, APC pretreatment, DNase I pretreatment, or nucleosomes stereotactic injection in mPFC were presented. **(G)** Representative flow cytometry images and statistical analysis showing the percentage of CD11b<sup>+</sup>CD45<sup>Low</sup>MHC-II<sup>+</sup> microglia on 3 days after ACSF, APC pretreatment, DNase I pretreatment, or nucleosomes stereotactic injection in mPFC were presented (two-way ANOVA with Tukey's *post hoc test* *post hoc*,  $^{***}P < 0.001$ , compared with ACSF;  $^{\#\#\#}P < 0.001$ , compared with APC;  $^{\#\#\#}P < 0.001$ , compared with DNase I;  $n = 6$ ). **(H)** Concentration of IL-1 $\beta$  on 3 days after ACSF, APC pretreatment, DNase I pretreatment, or nucleosomes stereotactic injection in mPFC was analyzed (two-way ANOVA with Tukey's *post hoc test* *post hoc*,  $^{***}P < 0.001$ , compared with ACSF;  $^{\#\#\#}P < 0.001$ , compared with APC;  $^{\#\#\#}P < 0.001$ , compared with DNase I;  $n = 6$ ).

Efforts have been made in the past decades to explore how stress alters microglial function (40, 41). Although it remains far from being revealed which signaling cascade initiates stress-triggered microglial changes, a surge of evidence indicates that several factors, including DAMPs signaling after stress exposure that augments the inflammatory responses, may be involved (42, 43). DAMPs are a variety of intracellular endogenous molecules that released to extracellular space during cellular stress and tissue damage and contribute to several of inflammatory diseases (44). Nowadays, it is largely accepted that DAMPs will initiate sterile immune-inflammation responses by inducing the activation of multiple classic pattern recognition receptors (PRRs), including membrane-bound TLRs and CLR,

cytoplasmic NLRs, and multiple intracellular DNA or RNA sensors, such as TLR3/7/9, cyclic GMP-AMP synthase, absent in melanoma 2, retinoic acid inducible gene I-like receptors, and melanoma differentiation-associated protein 5 (MDA5) (9, 45, 46). Moreover, DAMPs also can be recognized by several non-PRR DAMP receptors, including receptor for advanced glycation end products, triggering receptors expressed on myeloid cells, and several G-protein-coupled receptors and ion channels (47–50). Extracellular histones, damaged nucleosomes, and cell-free DNA are well-known nuclear DAMPs that efficiently induce inflammation, cytotoxicity, and tissue damage. More recently, extracellular histone-induced tissue damage and death have become hot issues of medical concern in sepsis, trauma,

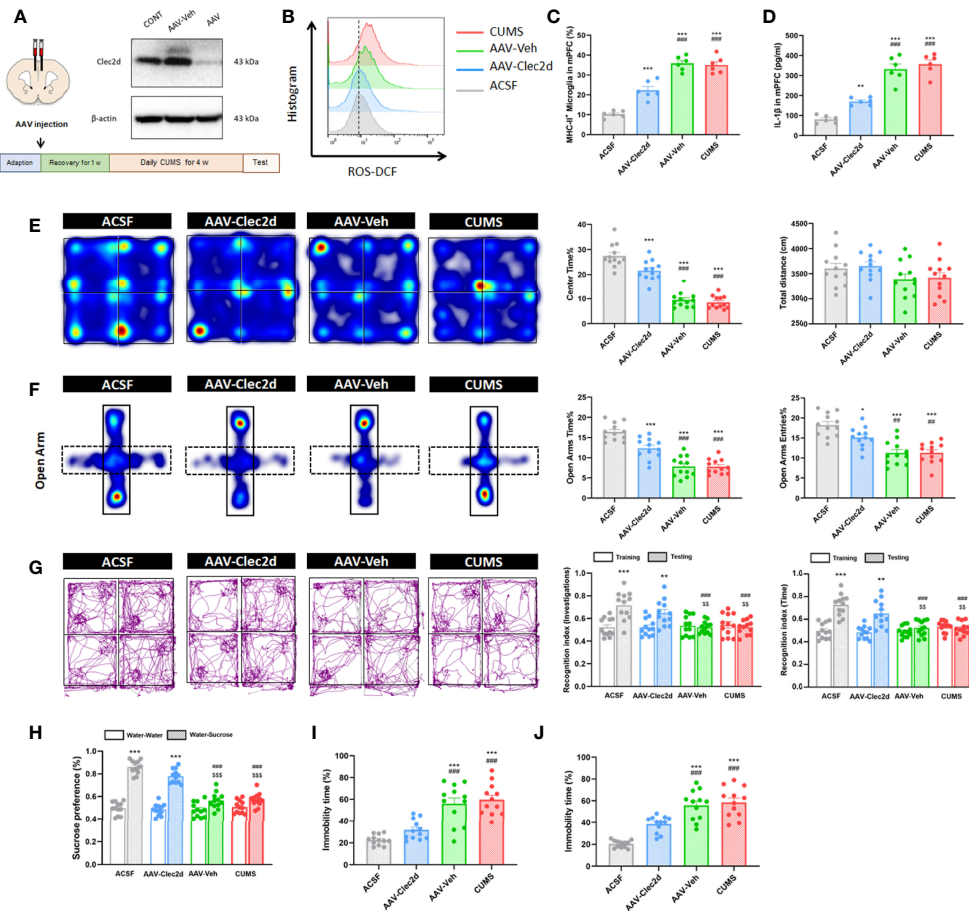


**FIGURE 8** | Clec2d knocking-down reduced microglial activation and inflammation in mPFC and improved negative emotional behaviors in mice with CUMS.

(A) Experimental protocol for mice receiving CUMS with Clec2d knocking-down in mPFC and representative Western blots showing the molecular expression were presented. (B) Representative histogram images showing CD11b<sup>+</sup>CD45<sup>LOW</sup> microglial ROS in mice receiving CUMS with Clec2d knocking-down in mPFC were presented. (C) The percentage of CD11b<sup>+</sup>CD45<sup>LOW</sup>MHC-II<sup>+</sup> microglia in mice receiving CUMS with Clec2d knocking-down in mPFC was analyzed (two-way ANOVA with Tukey's *post hoc* test *post hoc*, \*\*\**P* < 0.001, compared with ACSF; ###*P* < 0.001, compared with AAV-Clec2d; *n* = 6). (D) Concentration of IL-1β in mice receiving CUMS with Clec2d knocking-down in mPFC was analyzed (two-way ANOVA with Tukey's *post hoc* test *post hoc*, \*\**P* < 0.01, \*\*\**P* < 0.001, compared with ACSF; ###*P* < 0.001, compared with AAV-Clec2d; *n* = 6). (E) Representative heat maps for ACSF, AAV-Clec2d, AAV-Veh, and CUMS group in OF test were presented, and center time% and total distance were analyzed (two-way ANOVA with Tukey's *post hoc* test *post hoc*, \*\*\**P* < 0.001, compared with ACSF; ###*P* < 0.001, compared with AAV-Clec2d; *n* = 12). (F) Representative heat maps for ACSF, AAV-Clec2d, AAV-Veh, and CUMS group in EPMS test were presented, and open arm time% and open arm entries% were analyzed (two-way ANOVA with Tukey's *post hoc* test *post hoc*, \**P* < 0.05, \*\*\**P* < 0.001, compared with ACSF; ##*P* < 0.01, ###*P* < 0.001, compared with AAV-Clec2d; *n* = 12). (G) Representative trajectory images for ACSF, AAV-Clec2d, AAV-Veh, and CUMS group in NOR test were presented, and recognition index of investigations and time was analyzed (paired Student's *t*-test, \*\**P* < 0.01, \*\*\**P* < 0.001, compared with training. Two-way ANOVA with Tukey's *post hoc* test *post hoc*, ###*P* < 0.001, compared with ACSF-testing; \$\$\$*P* < 0.01, compared with AAV-Clec2d; *n* = 12). (H) Sucrose preference was analyzed (paired Student's *t*-test, \*\*\**P* < 0.001, compared with water-water, \*\*\*\**P* < 0.0001, compared with water-sucrose; ###*P* < 0.001, compared with ACSF-water-sucrose; \$\$\$*P* < 0.001, compared with AAV-Clec2d; *n* = 12). (I) Immobility time% in FS test was analyzed (two-way ANOVA with Tukey's *post hoc* test *post hoc*, \*\*\**P* < 0.001, compared with ACSF; ###*P* < 0.001, compared with AAV-Clec2d; *n* = 12). (J) Immobility time% in TS test was analyzed (two-way ANOVA with Tukey's *post hoc* test *post hoc*, \*\*\**P* < 0.001, compared with ACSF; ###*P* < 0.001, compared with AAV-Clec2d; *n* = 12).

ischemia/reperfusion (I/R) injury, and autoimmune diseases (51–55). There are three distinct extracellular forms of histone: free histones, DNA-bound histones (nucleosomes), and neutrophil extracellular traps (NET; webs of extracellular DNA decorated with histones, myeloperoxidase, and elastase). Although, remarkably, throughout current literatures, very little distinction among the presence of different forms of nuclear DAMPs in clinical samples is made, differing

significantly their mechanism of instigating inflammation and their cellular and molecular mediators should be identified. Free histones are unique cytotoxic DAMPs that elicit cytotoxicity dominantly through TLR-independent manner (14). Previous human observational studies indicated that the normal value of histones was reported to be about 0.06 ng/ml in serum. However, the levels would dramatically increase as high as 3 ng/ml in multiple trauma patients, and it was associated with

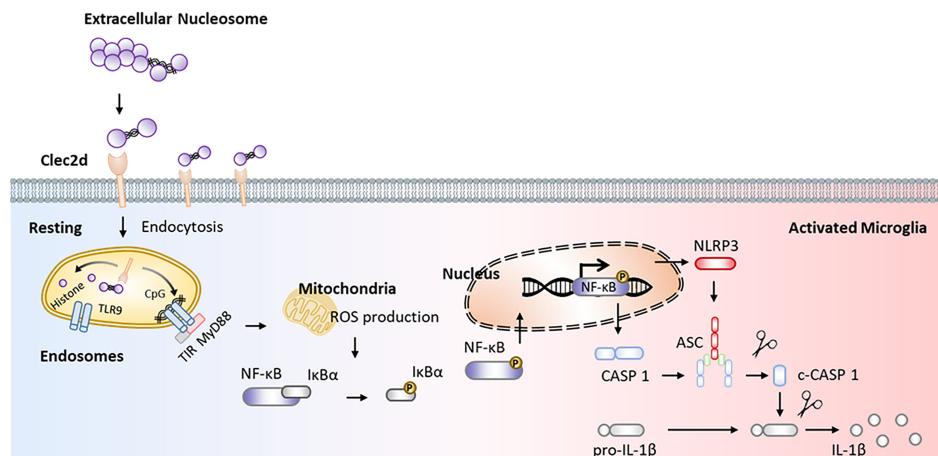


**FIGURE 9** | Graphical summary. Working model illustrating extracellular nucleosomes promoted microglial ROS production, primed NF- $\kappa$ B signaling pathway, and activated NLRP3 inflammasome via Clec2d and TLR9 in mPFC during chronic stress.

coagulopathy, endothelial damage and inflammation, organ dysfunction, and death in sepsis (23). Of note, a previous study reported that lesioned neutrophil-derived extracellular histones H4-mediated cytotoxicity disrupted and lysed the membrane of arterial smooth muscle cells, leading to the destabilization of atherosclerotic plaques (25). Besides, another study identified H1 as a major extracellular DAMPs that caused neurotoxicity within 24 h, even at a low concentration of 50 nM, while the other extracellular core histones H2A, H2B, H3, and H4 did not present neurotoxic at a concentration of 200 nM (24). However, the cytotoxicity induced by extracellular histones does not appear when extracellular histones bind with DNA. A study reported that injection of 1 mg purified nucleosomes did not provoke cytotoxicity in mice, although the saturation of the clearance mechanism had been reached, while injection of 1.25 mg of purified histones is lethal within 1 h in mice (22). Moreover, nucleosomes do not provoke cytotoxicity confirming *in vitro* that isolated nucleosomes did not induce cell death in cultured endothelial cells (13). Similarly, we also confirmed that all five recombinant histones (H1, H2A, H2B, H3, and H4) induced neuronal death at 10  $\mu$ g/ml (approximately 500 nM) indicated by decreased proportion of Calcein-AM<sup>+</sup> cells and increased of PI<sup>+</sup> cells, but not for nucleosomes, even at a relatively high concentration of 15  $\mu$ g/ml. However, the immuno-stimulation role and pro-inflammatory mechanism of extracellular nucleosomes *in vivo* have not been studied in large detail. Studies wherein incubated nucleosomes in human neutrophils and resulted in activation with upregulating of CD11b and promotion of phagocytosis. Interestingly, the study also indicated that the nucleosome-induced neutrophil activation was equally efficient in both wild-type and TLR2/4 knocking-down mice, indicating that a TLR2/4-independent pathway might be participated in nucleosome-induced inflammation (56, 57). Notably, Clec2d has been identified as a novel receptor that directly binds unmodified poly-basic regions on all histones (N-terminal tail of all histones and also C-

terminal tail of H1), providing a potential and attractive therapeutic target for extracellular histones-mediated inflammation and tissue damage. Besides, epigenetic regulation of histones modification also alters Clec2d to recognize them. Studies reported that lysine acetylation blocked recognition by Clec2d, and increasing histone acetylation by inhibiting histone deacetylases (HDAC) reduced the ability of injured cells to stimulate Clec2d (16, 58, 59). In the present study, we confirmed that nucleosomes did induce both Clec2d and TLR9 upregulation. Interestingly, the increase of intracellular Clec2d, especially in endosomes, was larger than that on the membrane, indicating an intracellular trafficking. It is worth noting that the stimulation of Clec2d with nucleosomes did not activate Syk, the downstream signaling kinase of activating CLRs, and Clec2d lacks of immunoreceptor tyrosine-based activation motifs or known signaling adaptors used by other activating CLRs, suggesting that Clec2d was not a signaling receptor. Besides, we only found detectable Clec2d-dependent activation of NF- $\kappa$ B instead of the other MAPKs, including p38, ERK, and JNK on both nucleosomes treatment wild-type and Clec2d knocking-down microglia. Moreover, the nucleosomes-induced microglial oxidative stress and inflammation were abolished in Clec2d knocking-down microglia. Considering that TLR9 is the dominant DNA sensor in endosomes, our results indicated that histones might deliver their bounded DNA to TLR9 in late endosomes to degrade by recognizing Clec2d and then priming TLR9-NF- $\kappa$ B pathway and activating ROS-NLRP3 inflammasome-dependent pro-inflammatory cytokine response. These findings were consistent with previous reports that endosomal TLRs are involved in histones-induced pathology.

There are several limitations in the study. First, extracellular traps, especially for NETs, were typically found in server trauma, sepsis, ischemia-reperfusion injury, cerebral stroke, disseminated intravascular coagulation, and multiple organ failure (14). However, it has not been described in mild stress such as

CUMS and CORT. This discrepancy might be derived from the intensity of stress. In the current study, we failed to provide more specific direct morphological evidence on microglial extracellular traps formation (MPO<sup>+</sup>DAPI<sup>+</sup> microglia) in mPFC and on primary microglia incubated with CORT in a physiological stress concentration (100, 200, 500, and 1,000 ng/ml) (60). The reason might be ascribed to CORT did not induce microglial NETosis. Second, the origin of extracellular nucleosomes is dying or a damaged cell; however, the mechanisms by which nucleosomes are released into the extracellular environment have not been studied in large detail. Existing evidence suggests that nucleosome release shares different mechanisms by different types of cell death, for example, apoptosis, necrosis, pyroptosis, necroptosis, and NETosis. For apoptosis, the active and passive release mechanism of nucleosome is dependent on caspase-activated DNase, as well as Factor VII-activating protease and Factor H activation, respectively (44, 61–63). In contrast to apoptosis, necrotic cell death does not involve the activity of intracellular nucleases but requires circulating nucleases (64). Moreover, in addition to the release of nucleosome/chromatin from dying non-myeloid cells, activated neutrophils (also been found in other cell types, for instance, mast cells, basophils, and macrophages) may undergo NETosis whereby their chromatin is excreted into the extracellular environment to form NETs by a PAD4 activation-dependent manner (65, 66). Third, although we showed the extracellular histones and nucleosomes in CSF, further study investigating nucleosomes secretion presenting in the blood sample of patients with depression will strengthen the relevance of the present study. Finally, the potential sex-specific effect is also needed in further study.

Taken together, our study revealed that extracellular nucleosomes promoted microglial ROS production, primed NF- $\kappa$ B signaling pathway, and activated NLRP3 inflammasome via Clec2d and TLR9 in mPFC during chronic stress. An elaborate understanding of the biology of microglial Clec2d on sensing extracellular nucleosomes and histones could be a novel therapeutic target for chronic stress-related emotional disorders.

## DATA AVAILABILITY STATEMENT

The raw data supporting the conclusions of this article will be made available by the authors, without undue reservation.

## REFERENCES

1. Troubat R, Barone P, Leman S, Desmidt T, Cressant A, Atanasova B, et al. Neuroinflammation and Depression: A Review. *Eur J Neurosci* (2021) 53 (1):151–71. doi: 10.1111/ejn.14720
2. Beurel E, Toups M, Nemeroff CB. The Bidirectional Relationship of Depression and Inflammation: Double Trouble. *Neuron* (2020) 107(2):234–56. doi: 10.1016/j.neuron.2020.06.002
3. Prinz M, Jung S, Priller J. Microglia Biology: One Century of Evolving Concepts. *Cell* (2019) 179(2):292–311. doi: 10.1016/j.cell.2019.08.053
4. Frank MG, Fonken LK, Watkins LR, Maier SF. Microglia: Neuroimmune-Sensors of Stress. *Semin Cell Dev Biol* (2019) 94:176–85. doi: 10.1016/j.semcdb.2019.01.001
5. Fu R, Shen Q, Xu P, Luo JJ, Tang Y. Phagocytosis of Microglia in the Central Nervous System Diseases. *Mol Neurobiol* (2014) 49(3):1422–34. doi: 10.1007/s12035-013-8620-6
6. Karadag H, Saygili G, Yuksel R, Usta MB, Topcuoglu C, Erzincan G. Serum TNF-Related Weak Inducer of Apoptosis (TWEAK), TNF-Related Apoptosis-Inducing Ligand (TRAIL) Levels in Patients With Bipolar Depression, Major Depression and a Healthy Control Group. *Psychiatr Danub* (2021) 33(3):314–9. doi: 10.24869/psyd.2021.314
7. Wiener CD, Moreira FP, Portela LV, Strogulski NR, Lara DR, da Silva RA, et al. Interleukin-6 and Interleukin-10 in Mood Disorders: A Population-Based Study. *Psychiatry Res* (2019) 273:685–9. doi: 10.1016/j.psychres.2019.01.100

## ETHICS STATEMENT

The animal study was reviewed and approved by Institutional Animal Care and Use Committee at Xiamen University.

## AUTHOR CONTRIBUTIONS

HW contributed to conceive the study, designed experiments, interpreted and analysis the data, and wrote the manuscript. HB, CL, QZ, AH, MQ, CHL, and YX conceived the study. GC and LH were the guarantor of this work and, as such, had full access to all data in the study and takes responsibility for the integrity of the data and the accuracy of the data analysis, as well as supervised the work and edited the manuscript. All authors have read and approved this manuscript prior to submission.

## FUNDING

This work is partly supported by National Natural Science Foundation of China (NSFC 81701091, 81870828, 81801101), Natural Science Foundation of Fujian Province (2020J01017), and Scientific Research Foundation for Personnel, Xiang'an Hospital of Xiamen University (PM201809170003). The funders had no role in study design, data collection and analysis, decision to publish, or preparation of the manuscript.

## ACKNOWLEDGMENTS

We gratefully acknowledge the help of the past and present members of the Central Laboratory, Xiang'an Hospital of Xiamen University for their great supports. Moreover, the authors would also like to thank Haiping Zheng, Xiang You, and Jingru Huang in the Core Facility of Biomedical, Xiamen University for their technical help in flow cytometry and confocal microscopy.

## SUPPLEMENTARY MATERIAL

The Supplementary Material for this article can be found online at: <https://www.frontiersin.org/articles/10.3389/fimmu.2022.854202/full#supplementary-material>

8. Lu J, Li S, Li H, Mou T, Zhou L, Huang B, et al. IL-1beta And Hypocretin In People Who Died By Suicide. *Neuropsychiatr Dis Treat* (2019) 15:2893–900. doi: 10.2147/NDT.S219962
9. Piccinini AM, Midwood KS. DAMPening Inflammation by Modulating TLR Signalling. *Mediators Inflammation* (2010) 2010:672395. doi: 10.1155/2010/672395
10. Donnelly CR, Chen O, Ji RR. How Do Sensory Neurons Sense Danger Signals? *Trends Neurosci* (2020) 43(10):822–38. doi: 10.1016/j.tins.2020.07.008
11. Halaris A. Inflammation and Depression But Where Does the Inflammation Come From? *Curr Opin Psychiatry* (2019) 32(5):422–8. doi: 10.1097/YCO.0000000000000531
12. Cheng Z, Abrams ST, Toh J, Wang SS, Wang Z, Yu Q, et al. The Critical Roles and Mechanisms of Immune Cell Death in Sepsis. *Front Immunol* (2020) 11:1918. doi: 10.3389/fimmu.2020.01918
13. Silk E, Zhao H, Weng H, Ma D. The Role of Extracellular Histone in Organ Injury. *Cell Death Dis* (2017) 8(5):e2812. doi: 10.1038/cddis.2017.52
14. Marsman G, Zeerleder S, Luken BM. Extracellular Histones, Cell-Free DNA, or Nucleosomes: Differences in Immunostimulation. *Cell Death Dis* (2016) 7(12):e2518. doi: 10.1038/cddis.2016.410
15. Del Fresno C, Sancho D. Clec2d Joins the Cell Death Sensor Ranks. *Immunity* (2020) 52(1):6–8. doi: 10.1016/j.immuni.2019.12.015
16. Lai JJ, Cruz FM, Rock KL. Immune Sensing of Cell Death Through Recognition of Histone Sequences by C-Type Lectin-Receptor-2d Causes Inflammation and Tissue Injury. *Immunity* (2020) 52(1):123–35. doi: 10.1016/j.immuni.2019.11.013
17. Nollet M, Le Guisquet AM, Belzung C. Models of Depression: Unpredictable Chronic Mild Stress in Mice. *Curr Protoc Pharmacol* (2013) 5:5.65. doi: 10.1002/0471141755.ph0565s61
18. Ding H, Cui XY, Cui SY, Ye H, Hu X, Zhao HL, et al. Depression-Like Behaviors Induced by Chronic Corticosterone Exposure via Drinking Water: Time-Course Analysis. *Neurosci Lett* (2018) 687:202–6. doi: 10.1016/j.neulet.2018.09.059
19. de Pablos RM, Herrera AJ, Espinosa-Oliva AM, Sarmiento M, Munoz MF, Machado A, et al. Chronic Stress Enhances Microglia Activation and Exacerbates Death of Nigral Dopaminergic Neurons Under Conditions of Inflammation. *J Neuroinflamm* (2014) 11:34. doi: 10.1186/1742-2094-11-34
20. Petrozziello T, Mills AN, Vaine CA, Penney EB, Fernandez-Cerado C, Legarda GPA, et al. Neuroinflammation and Histone H3 Citrullination Are Increased in X-Linked Dystonia Parkinsonism Post-Mortem Prefrontal Cortex. *Neurobiol Dis* (2020) 144:105032. doi: 10.1016/j.nbd.2020.105032
21. Thiam HR, Wong SL, Qiu R, Kittisopikul M, Vahabikashi A, Goldman AE, et al. NETosis Proceeds by Cytoskeleton and Endomembrane Disassembly and PAD4-Mediated Chromatin Decondensation and Nuclear Envelope Rupture. *Proc Natl Acad Sci U S A* (2020) 117(13):7326–37. doi: 10.1073/pnas.1909546117
22. Xu J, Zhang X, Pelayo R, Monestier M, Ammollo CT, Semeraro F, et al. Extracellular Histones Are Major Mediators of Death in Sepsis. *Nat Med* (2009) 15(11):1318–21. doi: 10.1038/nm.2053
23. Ekanev ML, Otto GP, Sosdorf M, Sponholz C, Boehringer M, Loesche W, et al. Impact of Plasma Histones in Human Sepsis and Their Contribution to Cellular Injury and Inflammation. *Crit Care* (2014) 18(5):543. doi: 10.1186/s13054-014-0543-8
24. Gilthorpe JD, Oozer F, Nash J, Calvo M, Bennett DL, Lumsden A, et al. Extracellular Histone H1 Is Neurotoxic and Drives a Pro-Inflammatory Response in Microglia. *Fl1000Res* (2013) 2:148. doi: 10.12688/fl1000research.2-148.v1
25. Silvestre-Roig C, Braster Q, Wichapong K, Lee EY, Teulon JM, Berrebeh N, et al. Externalized Histone H4 Orchestrates Chronic Inflammation by Inducing Lytic Cell Death. *Nature* (2019) 569(7755):236–40. doi: 10.1038/s41586-019-1167-6
26. Abrams ST, Zhang N, Dart C, Wang SS, Thachil J, Guan Y, et al. Human CRP Defends Against the Toxicity of Circulating Histones. *J Immunol* (2013) 191(5):2495–502. doi: 10.4049/jimmunol.1203181
27. Gauthier VJ, Tyler LN, Mannik M. Blood Clearance Kinetics and Liver Uptake of Mononucleosomes in Mice. *J Immunol* (1996) 156(3):1151–6.
28. Decker P, Wolburg H, Rammensee HG. Nucleosomes Induce Lymphocyte Necrosis. *Eur J Immunol* (2003) 33(7):1978–87. doi: 10.1002/eji.200323703
29. Kaufmann FN, Costa AP, Ghisleni G, Diaz AP, Rodrigues ALS, Peluffo H, et al. NLRP3 Inflammation-Driven Pathways in Depression: Clinical and Preclinical Findings. *Brain Behav Immun* (2017) 64:367–83. doi: 10.1016/j.bbi.2017.03.002
30. Meyer JH, Cervenka S, Kim MJ, Kreisl WC, Henter ID, Innis RB. Neuroinflammation in Psychiatric Disorders: PET Imaging and Promising New Targets. *Lancet Psychiatry* (2020) 7(12):1064–74. doi: 10.1016/S2215-0366(20)30255-8
31. Da Silva T, Hafizi S, Rusjan PM, Houle S, Wilson AA, Prce I, et al. GABA Levels and TSPO Expression in People at Clinical High Risk for Psychosis and Healthy Volunteers: A PET-MRS Study. *J Psychiatry Neurosci* (2019) 44(2):111–9. doi: 10.1503/jpn.170201
32. Hafizi S, Da Silva T, Meyer JH, Kiang M, Houle S, Remington G, et al. Interaction Between TSPO-A Neuroimmune Marker-and Redox Status in Clinical High Risk for Psychosis: A PET-MRS Study. *Neuropsychopharmacology* (2018) 43(8):1700–5. doi: 10.1038/s41386-018-0061-5
33. Setiawan E, Wilson AA, Mizrahi R, Rusjan PM, Miler L, Rajkowska G, et al. Role of Translocator Protein Density, a Marker of Neuroinflammation, in the Brain During Major Depressive Episodes. *JAMA Psychiatry* (2015) 72(3):268–75. doi: 10.1001/jamapsychiatry.2014.2427
34. Myers-Schulz B, Koenigs M. Functional Anatomy of Ventromedial Prefrontal Cortex: Implications for Mood and Anxiety Disorders. *Mol Psychiatry* (2012) 17(2):132–41. doi: 10.1038/mp.2011.88
35. Yarkoni T, Poldrack RA, Nichols TE, Van Essen DC, Wager TD. Large-Scale Automated Synthesis of Human Functional Neuroimaging Data. *Nat Methods* (2011) 8(8):665–70. doi: 10.1038/nmeth.1635
36. Hiser J, Koenigs M. The Multifaceted Role of the Ventromedial Prefrontal Cortex in Emotion, Decision Making, Social Cognition, and Psychopathology. *Biol Psychiatry* (2018) 83(8):638–47. doi: 10.1016/j.biopsych.2017.10.030
37. Savage JC, Carrier M, Tremblay ME. Morphology of Microglia Across Contexts of Health and Disease. *Methods Mol Biol* (2019) 2034:13–26. doi: 10.1007/978-1-4939-9658-2\_2
38. Bitzer-Quintero OK, Gonzalez-Burgos I. Immune System in the Brain: A Modulatory Role on Dendritic Spine Morphophysiology? *Neural Plast* (2012) 2012:348642. doi: 10.1155/2012/348642
39. Brown GC, Neher JJ. Microglial Phagocytosis of Live Neurons. *Nat Rev Neurosci* (2014) 15(4):209–16. doi: 10.1038/nrn3710
40. Calcia MA, Bonsall DR, Bloomfield PS, Selvaraj S, Barichello T, Howes OD. Stress and Neuroinflammation: A Systematic Review of the Effects of Stress on Microglia and the Implications for Mental Illness. *Psychopharmacol (Berl)* (2016) 233(9):1637–50. doi: 10.1007/s00213-016-4218-9
41. Ramirez K, Fornaguera-Trias J, Sheridan JF. Stress-Induced Microglia Activation and Monocyte Trafficking to the Brain Underlie the Development of Anxiety and Depression. *Curr Top Behav Neurosci* (2017) 31:155–72. doi: 10.1007/7854\_2016\_25
42. Frank MG, Weber MD, Watkins LR, Maier SF. Stress Sounds the Alarm: The Role of the Danger-Associated Molecular Pattern HMGB1 in Stress-Induced Neuroinflammatory Priming. *Brain Behav Immun* (2015) 48:1–7. doi: 10.1016/j.bbi.2015.03.010
43. Simpson DSA, Oliver PL. ROS Generation in Microglia: Understanding Oxidative Stress and Inflammation in Neurodegenerative Disease. *Antioxidants (Basel)* (2020) 9(8):743. doi: 10.3390/antiox9080743
44. Murao A, Aziz M, Wang H, Brenner M, Wang P. Release Mechanisms of Major DAMPs. *Apoptosis* (2021) 26(3-4):152–62. doi: 10.1007/s10495-021-01663-3
45. Gong T, Liu L, Jiang W, Zhou R. DAMP-Sensing Receptors in Sterile Inflammation and Inflammatory Diseases. *Nat Rev Immunol* (2020) 20(2):95–112. doi: 10.1038/s41577-019-0215-7
46. Mayer S, Raulf MK, Lepenies B. C-Type Lectins: Their Network and Roles in Pathogen Recognition and Immunity. *Histochem Cell Biol* (2017) 147(2):223–37. doi: 10.1007/s00418-016-1523-7
47. Huebener P, Pradere JP, Hernandez C, Gwak GY, Cavaglia JM, Mu X, et al. The HMGB1/RAGE Axis Triggers Neutrophil-Mediated Injury Amplification Following Necrosis. *J Clin Invest* (2015) 125(2):539–50. doi: 10.1172/JCI6887
48. Roe K, Gibot S, Verma S. Triggering Receptor Expressed on Myeloid Cells-1 (TREM-1): A New Player in Antiviral Immunity? *Front Microbiol* (2014) 5:627. doi: 10.3389/fmicb.2014.00627
49. Jimenez-Duran G, Triantafyllou M. Metabolic Regulators of Enigmatic Inflammation in Autoimmune Diseases and Crosstalk With Innate

- Immune Receptors. *Immunology* (2021) 163(4):348–62. doi: 10.1111/imm.13326
50. Santoni G, Cardinali C, Morelli MB, Santoni M, Nabissi M, Amantini C. Danger- and Pathogen-Associated Molecular Patterns Recognition by Pattern-Recognition Receptors and Ion Channels of the Transient Receptor Potential Family Triggers the Inflammasome Activation in Immune Cells and Sensory Neurons. *J Neuroinflamm* (2015) 12:21. doi: 10.1186/s12974-015-0239-2
  51. Li Y, Wan D, Luo X, Song T, Wang Y, Yu Q, et al. Circulating Histones in Sepsis: Potential Outcome Predictors and Therapeutic Targets. *Front Immunol* (2021) 12:650184. doi: 10.3389/fimmu.2021.650184
  52. Mao JY, Zhang JH, Cheng W, Chen JW, Cui N. Effects of Neutrophil Extracellular Traps in Patients With Septic Coagulopathy and Their Interaction With Autophagy. *Front Immunol* (2021) 12:757041. doi: 10.3389/fimmu.2021.757041
  53. Shah M, He Z, Rauf A, Kalkhoran SB, Heiestad CM, Stenslokken KO, et al. Extracellular Histones Are a Target in Myocardial Ischaemia Reperfusion Injury. *Cardiovasc Res* (2022) 118(4):1115–25. doi: 10.1093/cvr/cvab139
  54. Liu X, Arfman T, Wichapong K, Reutelingsperger CPM, Voorberg J, Nicolaes GAF. PAD4 Takes Charge During Neutrophil Activation: Impact of PAD4 Mediated NET Formation on Immune-Mediated Disease. *J Thromb Haemost* (2021) 19(7):1607–17. doi: 10.1111/jth.15313
  55. Eppensteiner J, Davis RP, Barbas AS, Kwun J, Lee J. Immunothrombotic Activity of Damage-Associated Molecular Patterns and Extracellular Vesicles in Secondary Organ Failure Induced by Trauma and Sterile Insults. *Front Immunol* (2018) 9:190. doi: 10.3389/fimmu.2018.00190
  56. Lindau D, Ronnefarth V, Erbacher A, Rammensee HG, Decker P. Nucleosome-Induced Neutrophil Activation Occurs Independently of TLR9 and Endosomal Acidification: Implications for Systemic Lupus Erythematosus. *Eur J Immunol* (2011) 41(3):669–81. doi: 10.1002/eji.201040593
  57. Ronnefarth VM, Erbacher AI, Lamkemeyer T, Madlung J, Nordheim A, Rammensee HG, et al. TLR2/TLR4-Independent Neutrophil Activation and Recruitment Upon Endocytosis of Nucleosomes Reveals a New Pathway of Innate Immunity in Systemic Lupus Erythematosus. *J Immunol* (2006) 177(11):7740–9. doi: 10.4049/jimmunol.177.11.7740
  58. Gange CT, Quinn JM, Zhou H, Kartsogiannis V, Gillespie MT, Ng KW. Characterization of Sugar Binding by Osteoclast Inhibitory Lectin. *J Biol Chem* (2004) 279(28):29043–9. doi: 10.1074/jbc.M312518200
  59. Kim SJ, Park JS, Lee DW, Lee SM. Trichostatin A Protects Liver Against Septic Injury Through Inhibiting Toll-Like Receptor Signaling. *Biomol Ther (Seoul)* (2016) 24(4):387–94. doi: 10.4062/biomolther.2015.176
  60. de Buhr N, von Kockritz-Blickwede M. Detection, Visualization, and Quantification of Neutrophil Extracellular Traps (NETs) and NET Markers. *Methods Mol Biol* (2020) 2087:425–42. doi: 10.1007/978-1-0716-0154-9\_25
  61. Radic M, Marion T, Monestier M. Nucleosomes Are Exposed at the Cell Surface in Apoptosis. *J Immunol* (2004) 172(11):6692–700. doi: 10.4049/jimmunol.172.11.6692
  62. Zeerleder S, Zwart B, te Velthuis H, Stephan F, Manoe R, Rensink I, et al. Nucleosome-Releasing Factor: A New Role for Factor VII-Activating Protease (FSAP). *FASEB J* (2008) 22(12):4077–84. doi: 10.1096/fj.08-110429
  63. Martin M, Leffler J, Smolag KI, Mytych J, Bjork A, Chaves LD, et al. Factor H Uptake Regulates Intracellular C3 Activation During Apoptosis and Decreases the Inflammatory Potential of Nucleosomes. *Cell Death Differ* (2016) 23(5):903–11. doi: 10.1038/cdd.2015.164
  64. Stephan F, Marsman G, Bakker LM, Bulder I, Stavenuiter F, Aarden LA, et al. Cooperation of Factor VII-Activating Protease and Serum DNase I in the Release of Nucleosomes From Necrotic Cells. *Arthritis Rheumatol* (2014) 66(3):686–93. doi: 10.1002/art.38265
  65. Goldmann O, Medina E. The Expanding World of Extracellular Traps: Not Only Neutrophils But Much More. *Front Immunol* (2012) 3:420. doi: 10.3389/fimmu.2012.00420
  66. Metzler KD, Goosmann C, Lubojemska A, Zychlinsky A, Papayannopoulos V. A Myeloperoxidase-Containing Complex Regulates Neutrophil Elastase Release and Actin Dynamics During NETosis. *Cell Rep* (2014) 8(3):883–96. doi: 10.1016/j.celrep.2014.06.044

**Conflict of Interest:** The authors declare that the research was conducted in the absence of any commercial or financial relationships that could be construed as a potential conflict of interest.

**Publisher's Note:** All claims expressed in this article are solely those of the authors and do not necessarily represent those of their affiliated organizations, or those of the publisher, the editors and the reviewers. Any product that may be evaluated in this article, or claim that may be made by its manufacturer, is not guaranteed or endorsed by the publisher.

Copyright © 2022 Wu, Bao, Liu, Zhang, Huang, Quan, Li, Xiong, Chen and Hou. This is an open-access article distributed under the terms of the Creative Commons Attribution License (CC BY). The use, distribution or reproduction in other forums is permitted, provided the original author(s) and the copyright owner(s) are credited and that the original publication in this journal is cited, in accordance with accepted academic practice. No use, distribution or reproduction is permitted which does not comply with these terms.